Patchy sticky hard spheres: Analytical study and Monte Carlo simulations

Riccardo Fantoni,[a] Domenico Gazzillo,[b] and Achille Giacometti[c]
Dipartimento di Chimica Fisica, Università di Venezia, S. Marta DD 2137, I-30123 Venezia, Italy

Mark A. Miller[d]
University Chemical Laboratory, Lensfield Road, Cambridge CB2 1EW, United Kingdom

Giorgio Pastore[e]
Dipartimento di Fisica Teorica, Università di Trieste, Strada Costiera 11, 34100 Trieste, Italy

(Received 26 July 2007; accepted 12 October 2007; published online 19 December 2007)

We consider a fluid of hard spheres bearing one or two uniform circular adhesive patches, distributed so as not to overlap. Two spheres interact via a "sticky" Baxter potential if the line joining the centers of the two spheres intersects a patch on each sphere, and via a hard sphere potential otherwise. We analyze the location of the fluid-fluid transition and of the percolation line as a function of the size of the patch (the fractional coverage of the sphere's surface) and of the number of patches within a virial expansion up to third order and within the first two terms ($C0$ and $C1$) of a class of closures Cn hinging on a density expansion of the direct correlation function. We find that the locations of the two lines depend sensitively on both the total adhesive coverage and its distribution. The treatment is almost fully analytical within the chosen approximate theory. We test our findings by means of specialized Monte Carlo simulations and find the main qualitative features of the critical behavior to be well captured in spite of the low density perturbative nature of the closure. The introduction of anisotropic attractions into a model suspension of spherical particles is a first step toward a more realistic description of globular proteins in solution. © *2007 American Institute of Physics*. [DOI: 10.1063/1.2805066]

I. INTRODUCTION

The idea of modeling fluids as systems of spherical particles with orientationally dependent attraction dates back at least as far as Boltzmann, who envisaged chemical attraction between atoms only when "their sensitive regions are in contact."[1] Models of this type, featuring patchy interactions, are currently experiencing renewed relevance in the context of colloidal and biological matter in contrast to their original conception in connection with fluids of atoms and small molecules.[2–17]

The new interest arises for various reasons. On the technological side, patchy particles give the possibility of designing self-assembling nanoscale devices through anisotropic decorations of the particle surface by means of organic or biological molecules.[13–15] Nature provides inspiration for what might be achieved in this area, a particularly elegant example being the self-assembly of virus capsids. These protein shells are monodisperse and highly symmetric and are composed of identical subunits. Simplified descriptions of icosahedral virus capsids are currently being formulated using spherical subunits with directional interactions[18,19] and the possibility of adopting similar schemes to self-assemble other target structures is being explored.[13] This level of organization inevitably requires a certain specificity in the interactions between the subunits as well as measures to prevent further aggregation of the assembled objects.

Less specific patchy interactions give rise to associating fluids containing a distribution of cluster sizes or extended gel-like networks. The key feature of such systems is a set of pointlike sites on the particle surface, leading to strongly directional bonding with a maximum of one bond per site.[3,8,10,11,16,17] This type of interaction has proven invaluable in elucidating the interplay between fluid-fluid and sol-gel transitions. One advantage of these models is that powerful analytical tools are available for them, such as Wertheim's thermodynamic perturbation theory,[20] which yields accurate results under experimentally realistic conditions.[21,22]

In contrast to these models with attractive spots, one can envisage particles that interact through larger attractive regions on their surface, for example, globular proteins with patches of hydrophobic (nonpolar) amino acids exposed at the surface. Isotropic potentials have been remarkably successful in modeling the phase diagrams of certain proteins,[23–25] but it seems that not all features of their coexistence curves can be properly explained by such simple interactions.[26] In this sort of system, it seems more appropriate to consider regions with short-range attractive forces[2,4–7,9,12] rather than site-site bonds. These attractive patches are capable of sustaining as many "bonds" as permitted by geometry. The size of the patch therefore becomes an important new parameter that does not arise in most work

[a]Electronic mail: rfantoni@unive.it.
[b]Electronic mail: gazzillo@unive.it.
[c]Electronic mail: achille@unive.it.
[d]Electronic mail: mam1000@cam.ac.uk.
[e]Electronic mail: pastore@ts.infn.it.

on associating fluids. We note, however, that for sufficiently narrow patches, the two models become essentially equivalent.

In the present work, we focus on a simple yet physical model which is a variation of those treated in Ref. 12. We consider uniform circular patches distributed on the surface of the sphere in such a way that they do not overlap. The patches are delimited by circles which can be defined by the associated solid angles. Two particles experience an adhesive attraction only when a patch on one sphere touches a patch on the other. The adhesion is of Baxter's type,[27] i.e., the attraction has infinitesimal range, acting only when the particles are exactly in contact, as described in the next section. This model has the advantage that it can be tackled with analytical tools, unlike most other models for which not even the isotropic analog bears this appealing feature. Various issues arise in this sort of model relating to the stability of the liquid phase with respect to crystalline solid phases, and these points have been studied in Refs. 28 and 29.

The integral equation theory of fluids with an angularly dependent pair potential is complicated by the fact that the pair distribution function is also angularly dependent.[30] In the general case one must appeal to the symmetries of the fluid (translational invariance, rotational invariance, invariance under permutation of like particles, and invariance under the symmetry operations of the individual particles and of the correlation functions) in order to simplify the problem.[31–33] In some cases, it is possible to factorize the angular dependence of the Ornstein–Zernike (OZ) equation. For example, the factorization for a fluid of dipolar particles has long been known[34] and in Ref. 35 it is shown how to solve the dipole-dipole angular distribution of attraction in the adhesive limit within the Percus–Yevick framework. However, the dipolar case hinges on exploiting a special property of this particular angular distribution that is particularly useful for the angular convolution in the OZ equation. In contrast, for an angular dependence with discontinuities, such as the circular patches treated here, any approach relying on a spherical harmonic expansion would prove a formidable task due to the large number of terms necessary to capture the discontinuities.

In the present model we therefore follow a different route based on two parallel and related schemes. We first perform a virial expansion up to the third virial coefficient. We then proceed to study a class of closures (denoted $C0$, $C1,\ldots$) which were proposed in Ref. 36 and are based on a density expansion of the direct correlation function. In particular, the zeroth-order term ($C0$) turns out to be equivalent to a modified mean spherical approximation, whereas the first-order ($C1$) is known to provide the correct third virial coefficient.[36] Within both schemes we study the thermodynamics, radial distribution function and percolation threshold, and compare with specialized Monte Carlo simulations which were recently devised to this aim.[37] By varying the size of the adhesive patches and by selecting between one patch and two diametrically opposite patches, we are able to investigate the roles of both the total surface coverage and the geometrical distribution of the adhesion. In both the one- and two-patch cases we can change smoothly between small sticky spots, capable of making only one bond each, and the isotropic adhesive sphere. We find that the position of the critical fluid-fluid transition line and the percolation threshold are both sensitive to the surface coverage. At fixed coverage, there is also a dependence on the way in which this adhesion is distributed.

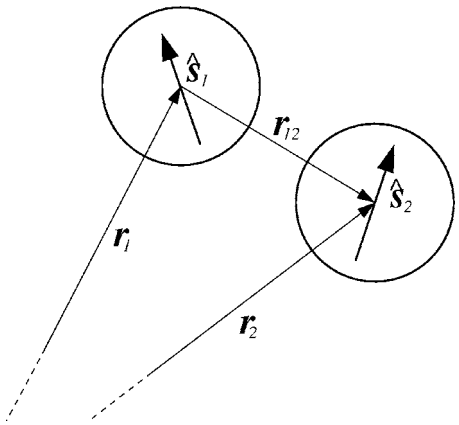

FIG. 1. Summary of the vector notation used to define the model.

Our results can be compared and contrasted with the recent work of Bianchi *et al.*,[17] who consider the maximum number of bonds per particle, rather than the fractional surface coverage, as the key parameter controlling the location of the critical point. In the present work we are able to tune both effects, thus illuminating their specific roles in the location of critical points.

The remainder of the paper is organized as follows. In Sec. II we introduce the model while Sec. III contains a description of the analytical and numerical tools used. Results for the radial distribution function, fluid-fluid transition, and percolation threshold are included in Secs. IV–VI, respectively. Finally, in Sec. VII the inclusion of an adhesive background is discussed, and conclusions and an outlook are contained in Sec. VIII.

II. DEFINITION OF THE MODEL

A. Baxter model with orientationally dependent adhesion

We start with some general remarks on the orientational dependence of a three-dimensional homogeneous fluid of hard spheres with adhesive pairwise interactions. Let $\mathbf{r}_i$ be the coordinates of the ith particle ($i=1,2,3,\ldots$) and assume that the patch distribution on the sphere has cylindrical symmetry so that its orientation in space is determined by a unit vector $\hat{\mathbf{s}}_i$ rigidly attached to it. Then $\hat{\mathbf{s}}_i=(\sin\theta_i\cos\varphi_i, \sin\theta_i\sin\varphi_i, \cos\theta_i)$ where θ_i and φ_i are the polar and the azimuthal angles with respect to a fixed reference frame (see Fig. 1). As usual, we introduce the relative coordinates $\mathbf{r}_{12}=\mathbf{r}_2-\mathbf{r}_1$ and the associated distance $r_{12}=|\mathbf{r}_{12}|$, and work with the following short-hand notation: $(1,2)=(\mathbf{r}_{12},\theta_1,\varphi_1,\theta_2,\varphi_2)$ and $\Omega_i=(\theta_i,\varphi_i)$ for the orientation of $\hat{\mathbf{s}}_i$. The orientation of $\hat{\mathbf{r}}_{ij}=\mathbf{r}_{ij}/r_{ij}$ with respect to the same frame of reference will be denoted by $\Omega_{ij}=(\theta_{ij},\varphi_{ij})$.

The particles interact through a pair potential $\phi(1,2)$,

defined later, which is a generalization of Baxter's sticky hard sphere (SHS) limit[27] to orientationally dependent interactions. We start with

$$\beta\Phi(1,2)=\begin{cases}+\infty & 0<r<\sigma\\ -\ln\left[\dfrac{\epsilon(1,2)}{12\tau}\dfrac{R}{R-\sigma}\right] & \sigma\le r\le R\\ 0 & r>R,\end{cases} \tag{1}$$

where $\beta=1/(k_BT)$ (k_B being Boltzmann's constant and T being the temperature), σ is the diameter of the spheres, and $\epsilon(1,2)/\tau$ is a dimensionless adhesion coefficient. We define $\phi(1,2)$ through the following limit on the Boltzmann factor e:

$$\begin{aligned}e(1,2)&=\exp[-\beta\phi(1,2)]\\&=\lim_{R\to\sigma}\exp[-\beta\Phi(1,2)]\\&=\Theta(r_{12}-\sigma)+\frac{\epsilon(1,2)}{\tau}\frac{\sigma}{12}\delta(r_{12}-\sigma),\end{aligned} \tag{2}$$

where $\Theta(\cdot)$ is the Heaviside step function and $\delta(\cdot)$ is the Dirac delta function. When $\epsilon(1,2)=1$ we recover the usual Baxter SHS model and, hence, the only orientational dependence is included in the definition of $\epsilon(1,2)$. It is easy to see that $\epsilon(1,2)$ cannot be a simple function of $\hat{\mathbf{s}}_1$ and $\hat{\mathbf{s}}_2$ but must also include a dependence on $\hat{\mathbf{r}}_{12}=\mathbf{r}_{12}/r_{12}$ in order to avoid a trivial corresponding states rescaling. This point is discussed in Appendix A. In the present work we shall address a type of orientational dependence which was introduced by Kern and Frenkel[12] following a previous suggestion by Jackson *et al.*[2]

B. Patchy sticky hard spheres

Consider a single hard sphere having one or more identical adhesive circular patches distributed on its surface in such a way that they do not overlap with one another. The size of the patch can be specified by the angular amplitude 2δ as shown in Fig. 2. The unit vector $\hat{\mathbf{s}}_i^{(p)}$ identifies the direction from the center of particle i to the center of patch p on the surface ($p=1,\ldots,n$, the total number of patches). The sticky area is then given by points $\hat{\mathbf{r}}$ on the surface of the particle such that the angle between $\hat{\mathbf{s}}_i^{(p)}$ and $\hat{\mathbf{r}}$ is smaller than δ.

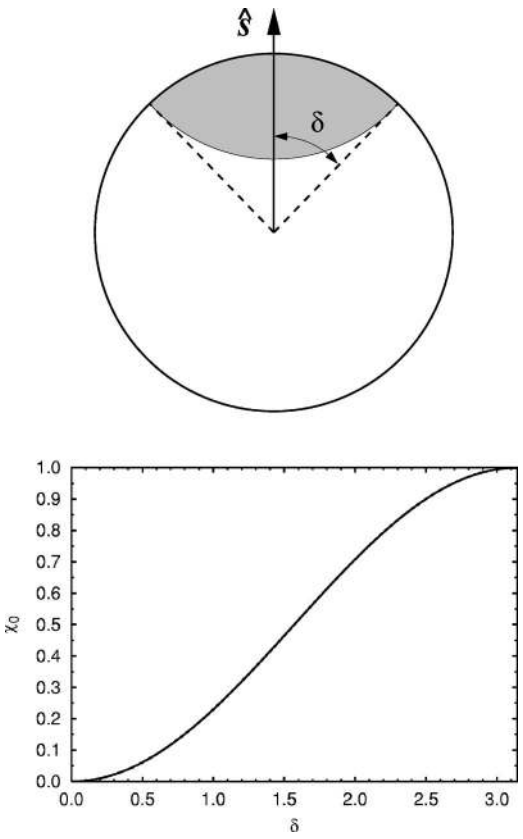

FIG. 2. Top panel: the adhesive patch model of Kern and Frenkel (Ref. 12). Bottom panel: patch surface coverage χ_0 as a function of the patch angle δ.

In conjunction with Eq. (2), the adhesive part of the interaction between two particles acts only if their point of contact lies inside a patch on each particle, as depicted in Fig. 3 for the case of a single patch ($n=1$). Therefore, $\epsilon(1,2)\equiv\epsilon(\hat{\mathbf{s}}_1,\hat{\mathbf{s}}_2,\hat{\mathbf{r}}_{12})$ can be written as

$$\epsilon(1,2)=\begin{cases}1 & \text{if } \hat{\mathbf{s}}_1^{(p_1)}\cdot\hat{\mathbf{r}}_{12}\ge\cos\delta \text{ and } -\hat{\mathbf{s}}_2^{(p_2)}\cdot\hat{\mathbf{r}}_{12}\ge\cos\delta \text{ for some combination } (p_1,p_2)\\ 0 & \text{otherwise.}\end{cases} \tag{3}$$

Each patch occupies a portion of the sphere's surface covered by the solid angle $2\pi(1-\cos\delta)$ and a fundamental role will be played in our discussion by the fraction of solid angle (i.e., the coverage) associated with δ, namely

$$\chi_0(\delta)=\frac{1}{2}(1-\cos\delta)=\sin^2\left(\frac{\delta}{2}\right). \tag{4}$$

III. ANALYSIS OF THE MODEL

A. Analytical solution

We now tackle the analytical solution of this problem based on two simple approximations: the virial expansion and the *C*n class of closures.

1. Virial expansion

As shown in Appendix B, the first two virial coefficients for this model are

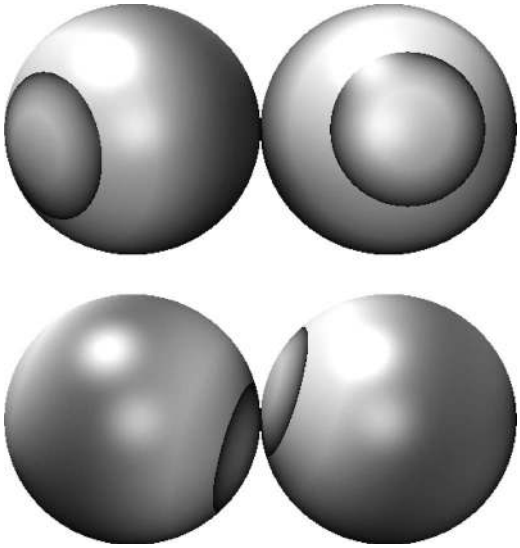

FIG. 3. Adhesion requires simultaneous alignment of patches (dark shading) on both spheres with the vector between their centers. The spheres in the upper panel do not adhere, while those in the lower panel do.

$$b_2 = B_2/v_0 = 4 - 12\frac{\chi_1}{12\tau}, \tag{5}$$

$$b_3 = B_3/v_0^2 = 10 - 60\frac{\chi_1}{12\tau} + 144\frac{\chi_2}{(12\tau)^2} - 96\frac{\chi_3}{(12\tau)^3}, \tag{6}$$

where $v_0 = \pi\sigma^3/6$ is the volume of a sphere and

$$\chi_2(\delta,n) = 4\left\langle \epsilon(1,3)\epsilon(2,3)\Theta\left(\frac{\pi}{3} - \theta_{13}\right)\right\rangle_{\Omega_1,\Omega_2,\Omega_3,\Omega_{13}}, \tag{8}$$

$$\chi_3(\delta,n) = \langle \epsilon(1,2)\epsilon(1,3)\epsilon(2,3)\rangle_{\Omega_1,\Omega_2,\Omega_3}\big|_{\theta_{12}=\pi/3,\,\theta_{23}=2\pi/3}, \tag{9}$$

where we have defined the angular average (with $d\tilde{\Omega} = d\Omega/4\pi$),

$$\langle \ldots \rangle_\Omega = \int d\tilde{\Omega} \ldots. \tag{10}$$

Here, θ_{ij} is the angle between $\hat{\mathbf{r}}_{ij}$ and $\hat{\mathbf{r}}_{13}$ (which can be chosen along the z axis), and $\epsilon(i,j)$ is always associated with a delta function that forces spheres i and j to be in contact. Note that in Eq. (6) the effect of anisotropy is embedded in the parameters χ_1, χ_2, χ_3 defined in Eqs. (7)–(9), and that these parameters are therefore functions of δ and n. The isotropic case is recovered when all χ's equal 1. We remark that the expression for χ_2 involves an average over the relative orientations Ω_{13} while there is an overlap between spheres 1 and 2, each of which is simultaneously in contact with sphere 3. Under such conditions there is always a maximum possible angle $\pi/3$ for θ_{13} and this gives rise to the normalization factor of 4 in Eq. (8).

If one limits the expansion to the second virial coefficient, a law of corresponding states based on the rescaling $\tau \to \tau/\chi_1$ between the patchy and the isotropic SHS models holds true. This correspondence breaks down even at the level of the third virial.

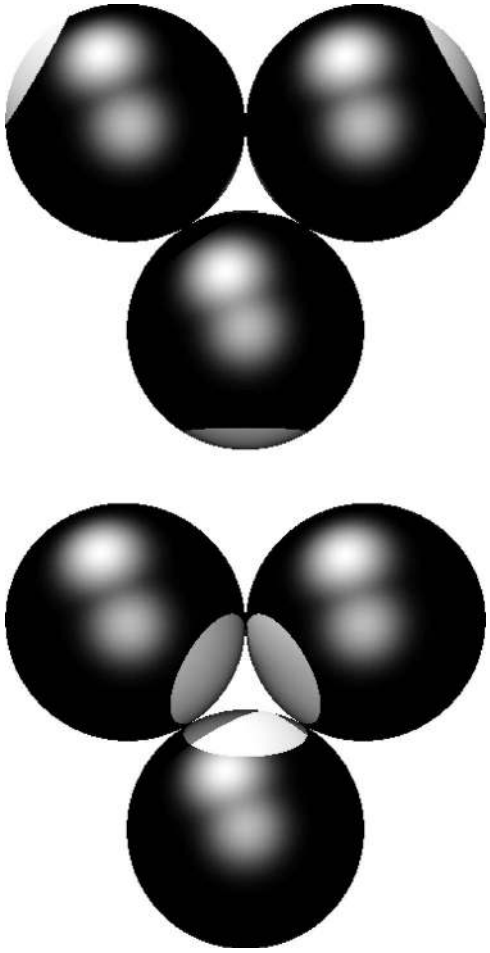

FIG. 4. Configurations of three mutually bonded spheres, each possessing a large single patch (dark shading). The patch vectors point inward in the top panel and outward in the bottom panel. The latter case is only possible for $\delta > 5\pi/6$. Combinations of these arrangements are also possible.

It is easy to see that $\chi_1 = n^2\chi_0^2$ as this is simply the product of the separate coverages on each sphere. A calculation of χ_2 and χ_3 is much more laborious and can be found in Appendix C for the case of a single patch. The final result in this case is

$$\chi_1 = \chi_0^2, \tag{11}$$

$$\chi_2 = \chi_0^2 Q_1(\delta), \tag{12}$$

$$\chi_3 = R_1^3(\delta), \tag{13}$$

where the coefficients Q_1 and R_1 are given in Appendix C. For $\delta \geq 5\pi/6$ it is possible to have three mutually bonded spheres with the patch vectors pointing either inward or outward (see Fig. 4). Note that for the isotropic limit $\delta = \pi$ all χ_i $(i=1,2,3)$ are equal to 1 as they should be. The three χ_i coefficients are plotted in Fig. 5 as functions of δ.

For spheres with two diametrically opposite patches, each of width δ, one finds

$$\chi_1 = 4\chi_0^2, \tag{14}$$

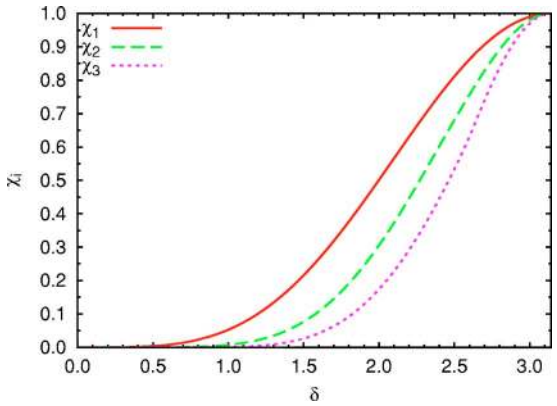

FIG. 5. (Color online) Dependence of the coefficients χ_i $(i=1,2,3)$ on δ for the one-patch model.

$$\chi_2 = 4\chi_0^2 Q_2(\delta), \tag{15}$$

$$\chi_3 = R_2^3(\delta), \tag{16}$$

where the coefficients Q_2 and R_2 are given in Appendix D. Note that in this case when $\delta > \pi/3$ it is also possible to have sphere 1 in contact with spheres 2 and 3 through different patches as shown in Fig. 6. The three χ_i coefficients are plotted in Fig. 7 as functions of δ.

The virial expansion of the excess free energy density is

$$\beta f^{\mathrm{ex}} v_0 = b_2\eta^2 + \tfrac{1}{2}b_3\eta^3 + \ldots, \tag{17}$$

where $\eta=\rho v_0$ is the hard sphere packing fraction. This allows the calculation of the corresponding pressure and chemical potential

$$\beta P(\tau,\eta)v_0 = \eta + b_2\eta^2 + b_3\eta^3 + \ldots,$$

$$\beta\mu(\tau,\eta) = \ln(\Lambda^3/v_0) + \ln\,\eta + 2b_2\eta + \tfrac{3}{2}b_3\eta^2 + \ldots,$$

where Λ is the de Broglie wavelength.

2. Integral equations within the Cn closures

While the virial expansion only allows a limited low-density region of the phase diagram to be probed, the integral equation approach is much more powerful in this respect. The trade-off is, of course, that since the OZ equation involves the total correlation function h and direct correlation function c, both of which are unknown, it can be solved only after adding a closure, that is a second, approximate, relationship involving h, c, and the pair potential. In this section we discuss a particular class of these closures (denoted Cn hereafter) which have already been exploited in the isotropic case and have proven to provide reasonably good predictions even for intermediate densities.[36]

The OZ equation for a homogeneous fluid of molecules interacting through anisotropic pair potentials is

$$h(1,2) = c(1,2) + \rho\int d(3)c(1,3)h(3,2), \tag{18}$$

where $d(i)\equiv d\mathbf{r}_i d\tilde{\Omega}_i$. More explicitly [see Eq. (10)],

$$h(1,2) = c(1,2) + \rho\int d\mathbf{r}_3\langle c(1,3)h(3,2)\rangle_{\Omega_3}. \tag{19}$$

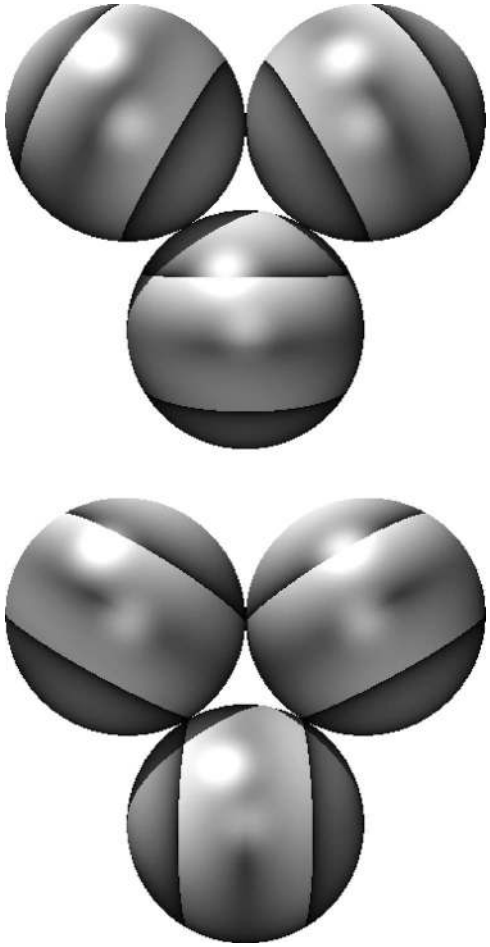

FIG. 6. Configurations of three mutually bonded spheres, each possessing two patches (dark shading). In the upper panel only one patch on each sphere is involved in the bonds; in the lower panel both patches on each sphere are involved. The latter case is only possible for $\delta \geq \pi/3$. Combinations of these arrangements are also possible.

In a homogeneous fluid, translational invariance of any correlation function implies that one can introduce reduced coordinates $\mathbf{r}_{12}=\mathbf{r}_2-\mathbf{r}_1$ and $\mathbf{r}_{13}=\mathbf{r}_3-\mathbf{r}_1$,

$$h(\mathbf{r}_{12},\Omega_1,\Omega_2) = c(\mathbf{r}_{12},\Omega_1,\Omega_2) + \rho\int d\mathbf{r}_3\langle c(\mathbf{r}_{13},\Omega_1,\Omega_3)h(\mathbf{r}_{32},\Omega_3,\Omega_2)\rangle_{\Omega_3}. \tag{20}$$

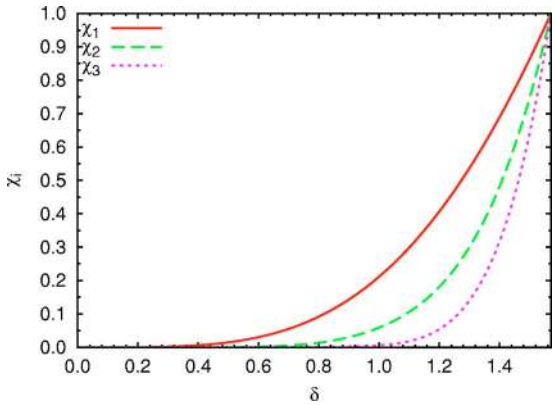

FIG. 7. (Color online) Dependence of the coefficients χ_i $(i=1,2,3)$ on δ for the two-patch model.

The presence of the convolution makes it convenient to Fourier transform this equation with respect to the position variable **r**. This yields for the corresponding functions (indicated with a hat) in Fourier space **k**,

$$\hat{h}(\mathbf{k},\Omega_1,\Omega_2) = \hat{c}(\mathbf{k},\Omega_1,\Omega_2) + \rho\langle\hat{c}(\mathbf{k},\Omega_1,\Omega_3)\hat{h}(\mathbf{k},\Omega_3,\Omega_2)\rangle_{\Omega_3}. \tag{21}$$

The additional complication with respect to the isotropic case is the presence of the orientational average of the product appearing in Eq. (21). In order to make progress, we use a simple angular decoupling approximation

$$\langle\hat{c}(\mathbf{k},\Omega_1,\Omega_3)\hat{h}(\mathbf{k},\Omega_3,\Omega_2)\rangle_{\Omega_3} \simeq \langle\hat{c}(\mathbf{k},\Omega_1,\Omega_3)\rangle_{\Omega_3}\langle\hat{h}(\mathbf{k},\Omega_3,\Omega_2)\rangle_{\Omega_3}. \tag{22}$$

As discussed in Ref. 36, *C*n closures are based on a density expansion of the cavity function $y(1,2)$ which is related to the radial distribution function $g(1,2)$ by $g(1,2)=y(1,2)e(1,2)$.

In the presence of anisotropy, all correlation functions clearly depend upon the solid angles $\Omega_1,\Omega_2,\Omega_{12}$. It is then customary to consider[30] the corresponding angular averaged quantities $g(r\equiv r_{12})=\langle g(1,2)\rangle_{\Omega_1,\Omega_2,\Omega_{12}}$ and similarly for $y(r\equiv r_{12})$. Within *C*n closures, for $r>\sigma$, the radial distribution function $g(r)$ coincides with the cavity function $y(r)$. A density expansion of the cavity function yields

$$y(r) = 1 + \rho y_1(r) + \ldots, \tag{23}$$

where

$$y_1(r_{12}) = \int d\mathbf{r}_3\langle f(1,3)f(3,2)\rangle_{\Omega_1,\Omega_2,\Omega_3,\Omega_{12}}. \tag{24}$$

Calculation of Eq. (24) proceeds using arguments akin to those presented in Appendix B, which are based on the decomposition in Eq. (B2). The integral in Eq. (24) then splits into three integrals containing the various combinations of the HS and the sticky parts of the Mayer function as in Eq. (B2).

B. Monte Carlo algorithms for Baxter-like potentials

Monte Carlo simulations of adhesive hard spheres require particular care even in the isotropic case because of the singular nature of the potential. For completeness we summarize the main ideas below, deferring to Ref. 37 for the details.

Conventional Monte Carlo displacements of a SHS would fail because the bonded states between particles occupy an infinitesimal volume of configuration space (and so would never be located by random displacements) but have infinite strength (and so would never be broken). The solution is to compare the integrated weights of the various bonded and unbonded states, which are finite. Specialized algorithms that exploit this approach have been devised for the canonical ensemble[38,39] and were subsequently extended to the grand canonical ensemble.[40,41] The latter is particularly convenient for identifying the critical point.[42]

The Monte Carlo algorithm for isotropic adhesive spheres can be modified to deal with the patchy case by incorporating the anisotropy in the acceptance criterion for trial moves. Trial moves are attempted as described in detail in Ref. 41 as though the spheres were uniformly adhesive. Once the trial position of the displaced particle has been chosen, a uniformly distributed random orientation is selected. The move is then accepted only if an overlap of hard cores is not generated (as in the isotropic case) and if all contacts specified in the trial configuration have patches suitably aligned to make the required bonds. This scheme produces the desired Boltzmann distribution[37] and is applicable to an arbitrary arrangement of patches. However, it becomes inefficient when the total adhesive coverage of the sphere is small because the random generation of orientations is then unlikely to lead to patches being aligned with bonds, leading to a high rejection rate.

IV. STRUCTURE

In the following we shall compare predictions from the combined *C*1-orientational mean field approximation and virial expansion with the results of Monte Carlo simulations.

One finds that $y_1(r)$ is different from zero only in the region $0\le r\le 2\sigma$ and

$$y_1(r) = \frac{\pi}{12}\left(\frac{r}{\sigma}+4\right)\left(\frac{r}{\sigma}-2\right)^2 + \frac{\chi_1}{12\tau}2\pi\left(\frac{r}{\sigma}-2\right) + \frac{\bar{\bar{\chi}}_2(r)}{(12\tau)^2}2\pi\frac{\sigma}{r}, \tag{25}$$

where

$$\bar{\bar{\chi}}_2(r) = \langle\epsilon(1,2)\epsilon(1,3)\rangle_{\Omega_1,\Omega_2,\Omega_3}\big|_{\theta_{12}=2\arcsin(r/2\sigma)}. \tag{26}$$

In order to compute the angularly averaged radial distribution function $g(r)$ we have solved the full OZ Eq. (20) within the *C*1 closure supplemented with the decoupling approximation (22). The Wertheim–Baxter method[27] and the *C*1 closure combine such that only the cavity function at contact depends upon the angular coefficients χ_1,χ_2,χ_3. The solution for Baxter function is

$$q(r) = [a(r^2-\sigma^2)/2 + b\sigma(r-\sigma) + q_\sigma\sigma^2]\Theta(\sigma-r) \quad r>0, \tag{27}$$

where

$$a = \frac{1+2\eta}{(1-\eta)^2} - \frac{12q_\sigma\eta}{1-\eta}, \tag{28}$$

$$b = -\frac{3\eta}{2(1-\eta)^2} + \frac{6q_\sigma\eta}{1-\eta}, \tag{29}$$

$$q_\sigma = \frac{\bar{y}^{C1}}{12\tau}, \tag{30}$$

$$\bar{y}^{C1} = \langle y^{C1}(r_{12}=\sigma,\Omega_1,\Omega_2,\Omega_{12})\epsilon(1,2)\rangle_{\Omega_1,\Omega_2,\Omega_{12}} = y_0 + y_1\eta. \tag{31}$$

The coefficients $y_{0,1}=y_{0,1}(\tau)$ are related to the reduced virial

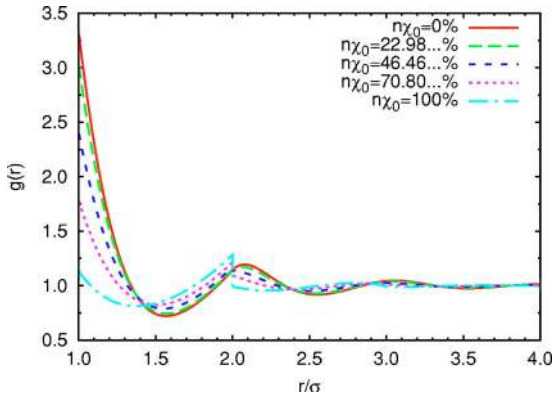

FIG. 8. (Color online) Radial distribution function for the one-patch model ($n=1$) at $\eta=0.4$ and $\tau=0.2$ within the $C1$ approximation and for various values of the adhesive coverage $n\chi_0$.

coefficients $b_{2,3}$ by Eq. (41), later. Therefore, we can read off their values

$$y_0 = \chi_1, \tag{32}$$

$$y_1 = \left(30\frac{\chi_1}{12\tau} - 144\frac{\chi_2}{(12\tau)^2} + 144\frac{\chi_3}{(12\tau)^3}\right)\tau. \tag{33}$$

In order to extract the numerical behavior of the radial distribution function $g(r)$ we have employed a discretization method due to Perram[43] to compute the numerical integral

$$rh(r) = -q'(r) + 2\pi\rho\int_0^\infty du\, q(u)(r-u)h(|r-u|). \tag{34}$$

For the one-patch spheres the result is reported in Fig. 8 for various values of δ, at $\eta=0.4$ and $\tau=0.2$. The choices $\delta=0$ and $\delta=\pi$ correspond to the limiting cases of pure HS and isotropic SHS, respectively. Upon decreasing the size of the patch, the behavior smoothly interpolates between these two cases, as expected. The characteristic jump in $g(r)$ at $r=2\sigma$ in the isotropic SHS model[41] can be explicitly computed within the $C1$ integral equation closure to be

$$g(2\sigma^+) - g(2\sigma^-) = -6\eta[\bar{y}^{C1}/(12\tau)]^2. \tag{35}$$

The jump is also present for intermediate values of δ and gradually fades out toward the HS result as illustrated in Fig. 8. In order to assess the precision of the predictions of the Cn closures, in Fig. 9 we compare the radial distribution generated by both $C0$ and $C1$ closures with Monte Carlo simulations (lower panel) and with the corresponding isotropic case (upper panel). The $C1$ closure is seen to follow the Monte Carlo behavior well over the range of the ratio r/σ considered, in both the isotropic and anisotropic cases.

Like the Percus–Yevick solution of the isotropic model, the $C0$ and $C1$ closures fail to capture certain δ function and step discontinuities in the radial distribution function,[44] such as those visible in the Monte Carlo results in the range $\sigma < r < 2\sigma$ in Fig. 9. These features arise from clusters in which the distance between two particles is fixed or limited indirectly by a sequence of adhesive bonds, for example, the outermost pair of particles in face-sharing tetrahedra. These clusters are sampled correctly by the Monte Carlo simulations.[45]

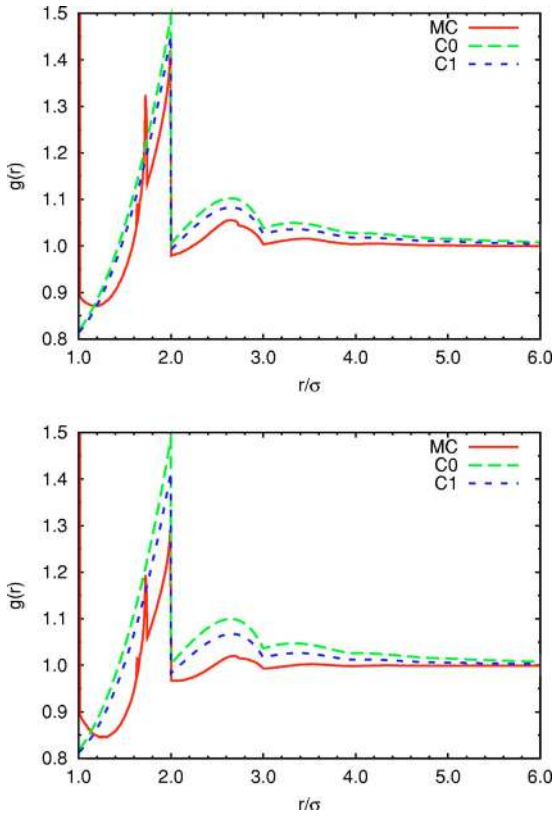

FIG. 9. (Color online) Comparison between the radial distribution function from MC simulations and from the $C0$ and $C1$ approximations in the isotropic case ($n\chi_0=100\%$, top panel) and for an intermediate value of the single patch ($n=1$) case with $n\chi_0=80\%$ (bottom panel). Both sets of calculations were performed at $\tau/(n\chi_0)^2=0.125$ and $\rho\sigma^3=0.35$ corresponding to $\eta=0.183\ldots$.

V. FLUID-FLUID COEXISTENCE CURVE

An interesting issue, both from the theoretical view point and for the possible implications in predictions of experimental phase transitions in solutions of globular proteins, is the determination of the fluid-fluid coexistence curve for the patchy sticky hard spheres, which we now address. We note that the dense fluid (liquid) phase, though often long-lived, is generally only metastable for systems of particles interacting through sufficiently short-ranged isotropic attractive forces. However, it has recently been predicted that a thermodynamically stable liquid will be recovered if the coordination number of the particles is restricted to a maximum of 6 or less.[29] Nevertheless, it seems that the specific details of the interactions must be taken into account before a firm conclusion can be drawn for a particular model.[46]

A. Virial expansion

In order to find the coexistence or binodal line we need to solve for $\eta_1(\tau)$ and $\eta_2(\tau)$ the following set of equations:

$$P(\tau,\eta_1) = P(\tau,\eta_2),$$

$$\mu(\tau,\eta_1) = \mu(\tau,\eta_2).$$

A straightforward use of Eq. (17) for the excess free energy density to this aim, however, yields meaningless results even at moderate densities as one could have expected

from the outset. A way out of this problem was proposed in Ref. 47 in the context of polydisperse SHS fluids. The idea hinges on a modification of the Carnahan–Starling expression for the HS excess free energy density[48]

$$\beta f_{\mathrm{cs}}^{\mathrm{ex}} v_0 = \frac{4-3\eta}{(1-\eta)^2}\eta^2, \tag{36}$$

so that it matches the patchy SHS result up to the third order in density. A possible choice is

$$\beta f^{\mathrm{ex}} v_0 = (c-1)\eta \ln(1-\eta) + 3d\frac{\eta^2}{1-\eta} + c\frac{\eta^2}{(1-\eta)^2}, \tag{37}$$

where c and d are parameters to be determined by expanding to the third order in density and matching to Eq. (17). We then find

$$c = \frac{b_3 - 2b_2 + 1}{3}, \tag{38}$$

$$d = \frac{b_2 - 1}{3}. \tag{39}$$

The pressure and the chemical potential are then

$$\beta P v_0 = \eta + \eta^2 \frac{1 + 3d(1-\eta) + \eta[\eta - 2 + c(3-\eta)]}{(1-\eta)^3},$$

$$\beta\mu = \ln(\Lambda^3/v_0) + \ln\,\eta + (c-1)\ln(1-\eta) + \frac{(1+c+6d)\eta - (2-2c+9d)\eta^2 + (1-c+3d)\eta^3}{(1-\eta)^3},$$

respectively. In the limit $c=d=1$ Eq. (37) reduces to Eq. (36) as expected.

The behavior of the binodal line as a function of δ is shown in Fig. 10. As δ decreases, the coexistence region shrinks as expected, since HS fluids ($\delta=0$) admit only a single phase.[49]

B. *C*1 integral equation

An alternative route is to start from the excess free energy stemming from the energy route of the $C1$ approximation[36]

$$\beta f^{\mathrm{ex}} v_0 = \beta f_{\mathrm{cs}}^{\mathrm{ex}} v_0 - (b_2 - b_2^{\mathrm{HS}})\eta^2 + (b_3 - b_3^{\mathrm{HS}})\frac{\eta^3}{2}, \tag{40}$$

where $b_n^{\mathrm{HS}} = b_n(\tau\to\infty)$. The rescaled virial coefficients $b_n = b_n(\tau)$ can be related to the values of the corresponding coefficients of the expansion for the cavity function at contact $\bar{y} = y_0 + y_1\eta + y_2\eta^2 + \ldots$ by means of the relation (see, e.g., Ref. 36, and references therein)

$$y_{n-2}(\tau)/\tau^2 = \frac{1}{n-1}\frac{d[b_n(\tau) - b_n^{\mathrm{HS}}]}{d\tau}, \quad n \geq 2. \tag{41}$$

Hence, we have

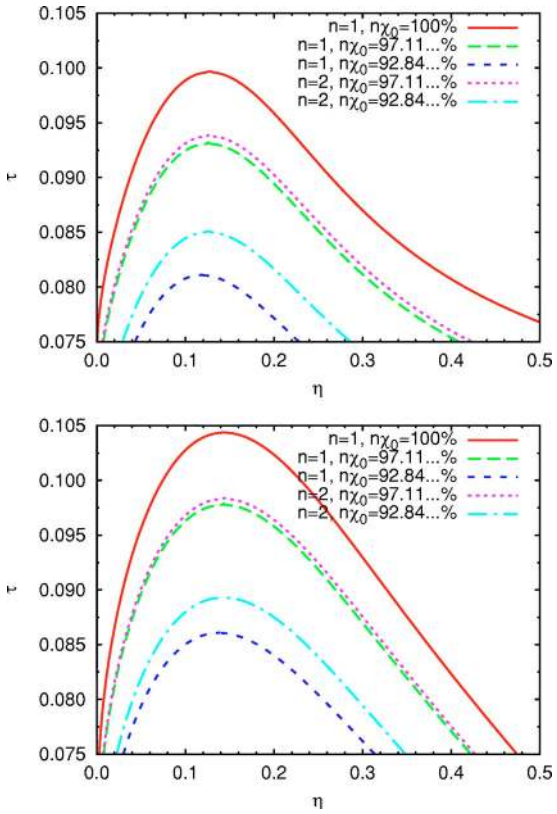

FIG. 10. (Color online) Dependence on the adhesive coverage $n\chi_0$ of the binodal line calculated from the modified Carnahan–Starling free energy of Eq. (37) (top panel) and from the $C1$ approximation of Eq. (40) (bottom panel). The one-patch ($n=1$) and two-patch ($n=2$) systems are compared at the same total coverage.

$$\beta P v_0 = \eta + 2\eta^2\frac{\eta-2}{(\eta-1)^3} - \frac{\chi_1}{\tau}\eta^2 + \left(-5\frac{\chi_1}{\tau} + \frac{\chi_2}{\tau^2} - \frac{1}{18}\frac{\chi_3}{\tau^3}\right)\eta^3, \tag{42}$$

$$\beta\mu = \ln(\Lambda^3/v_0) + \ln\,\eta + \eta\frac{8 + 3(\eta-3)\eta}{(1-\eta)^3} - \frac{\chi_1}{\tau}2\eta + \left(-5\frac{\chi_1}{\tau} + \frac{\chi_2}{\tau^2} - \frac{1}{18}\frac{\chi_3}{\tau^3}\right)\frac{3\eta^2}{2}. \tag{43}$$

We remark that these results need no further orientational approximations as all effects of anisotropy are exactly included in $\chi_{1,2,3}$.

The results for the binodals are shown in Fig. 10. For each of the adhesive coverages depicted, both theoretical treatments predict that the binodal line for the two-patch model lies above its counterpart for a single patch. This could be expected on physical grounds, since a more distributed region of adhesion usually facilitates the aggregation process. A closer analysis, however, indicates that this is not always the case. This is shown in Fig. 11 where we report the change in the critical point as a function of the adhesive coverage $n\chi_0$ of the sphere surface. The difference between one and two patches decreases as δ increases, as expected, but it is clearly visible through the whole range of existence. Remarkably, there is an inversion of the two curves around

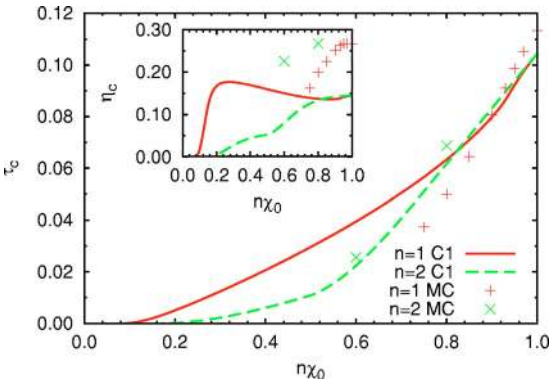

FIG. 11. (Color online) Dependence of the critical reduced temperature on the total adhesive coverage $n\chi_0$ for $n=1$ and 2 patches, calculated from the $C1$ approximation of Eq. (40) and from MC. The inset shows the critical packing fraction.

80% coverage. For approximately $n\chi_0 \geq 0.8$ the critical temperature for two patches lies above its one-patch counterpart. This means that the fluid-fluid transition line is encountered at higher temperature when an identical adhesive coverage is distributed over two spots rather than consolidated into a single big patch. However, this is no longer true when the size of the patch becomes too small. The reason is that under such conditions, it is then possible to bind three or more particles within a single patch, whereas at most two particles (one on each of the two opposite patches) can be attached in the two-patch case.

An additional noteworthy feature of Fig. 11 is the existence of a kink at $\delta=\pi/3$ (50% coverage) in the two-patch case. The kink is related to the degeneracy illustrated in Fig. 6. A similar kink occurs in the single-patch curve at $\delta=5\pi/6$ (93.3% coverage). Again, this stems from degeneracy, as illustrated in Fig. 4.

Due to the inherent difficulty of tracing out critical temperatures to low coverage, we have been unable to verify the crossing of the one- and two-patch critical temperatures by Monte Carlo (MC) simulations. Figure 11 reports MC results down to around 60% coverage and the two-patch critical temperature is always above the one-patch case. We suspect, however, that an inversion might still occur in MC simulations, but at lower values of χ_0, as yet inaccessible to our simulations.

The sensitivity of the shape and location of the coexistence curve to the geometry of the adhesive distribution is quite a remarkable feature of this archetypal patchy model. It seems likely, therefore, that a proper understanding of experimentally determined phase diagrams of globular proteins should take into account the nonuniformity of their surfaces and consequently of their interactions.

VI. PERCOLATION

A further interesting issue, already discussed in the context of the isotropic model, is the percolation threshold,[42,50] to which we now turn.

A. Virial expansion

In one-patch systems only dimers can form for δ up to $\pi/6$, while clusters of any size are in principle possible above this threshold. In order to study the percolation threshold we can use the strategy devised in Ref. 51. Based on the definition of the connectedness correlation function (see later), the percolation threshold is signaled by the divergence of the mean cluster size

$$S = 1 + \rho \int d\mathbf{r}_{12} \langle h^+(\mathbf{r}_{12},\Omega_1,\Omega_2)\rangle_{\Omega_1,\Omega_2}, \tag{44}$$

where h^+ is the pair connectedness function, which is related to the direct connectedness function c^+ by the Ornstein–Zernike equation. Both are related to the connected part of the Mayer function $f^+(1,2)=f(1,2)-f_{\mathrm{HS}}(1,2)$ as given in Eq. (B2), $f_{\mathrm{HS}}(1,2)$ being the HS part as given by Eq. (B3). As in the case of Eq. (22) we assume that

$$\langle \hat{c}^+(\mathbf{k},\Omega_1,\Omega_3)\hat{h}^+(\mathbf{k},\Omega_3,\Omega_2)\rangle_{\Omega_3} \simeq \langle \hat{c}^+(\mathbf{k},\Omega_1,\Omega_3)\rangle_{\Omega_3}\langle \hat{h}^+(\mathbf{k},\Omega_3,\Omega_2)\rangle_{\Omega_3}. \tag{45}$$

The average Fourier transform of the direct connectedness function $\hat{c}^+(k)=\langle \hat{c}^+(k,\Omega_1,\Omega_2)\rangle_{\Omega_1,\Omega_2}$ at $k=0$ then identifies the threshold by the equation

$$\rho\hat{c}^+(0) = 1. \tag{46}$$

Upon power expansion in the density we have

$$\hat{c}^+(0) = \sum_{n=2}^{\infty} \hat{c}_n^+(0)\rho^{n-2} = \hat{c}_2^+(0) + \rho\hat{c}_3^+(0) + O(\rho^2). \tag{47}$$

Using the earlier decomposition of the Mayer function the first two coefficients are found to be

$$\hat{c}_2^+(0) = \int d\mathbf{r}_{12}\langle f^+(1,2)\rangle_{\Omega_1,\Omega_2}, \tag{48}$$

$$\hat{c}_3^+(0) = \int d\mathbf{r}_{12}d\mathbf{r}_{13}\langle [f^+(1,2)f_{\mathrm{HS}}(1,3)f_{\mathrm{HS}}(2,3) + 3f_{\mathrm{HS}}(1,2)f^+(1,3)f^+(2,3) + f^+(1,2)f^+(1,3)f^+(2,3)]\rangle_{\Omega_1,\Omega_2,\Omega_3}. \tag{49}$$

An analysis following that in Appendix B then yields

$$\hat{c}_2^+(0)/v_0 = 24\frac{\chi_1}{12\tau}, \tag{50}$$

$$\hat{c}_3^+(0)/v_0^2 = 60\frac{\chi_1}{12\tau} - 432\frac{\chi_2}{(12\tau)^2} + 288\frac{\chi_3}{(12\tau)^3}. \tag{51}$$

To first order in the density, the percolation threshold is then given by a straight line

$$\tau = 2\chi_1\eta. \tag{52}$$

The next order already yields a more complex solution involving both χ_2 and χ_3,

$$\eta = \frac{-6\chi_1\tau^2 + \sqrt{6}\tau^{3/2}\sqrt{\chi_3 + 6\chi_1^2\tau - 18\chi_2\tau + 30\chi_1\tau^2}}{\chi_3 - 18\chi_2\tau + 30\chi_1\tau^2}. \quad (53)$$

We then see that for $\eta_- \leq \eta \leq \eta_+$ with

$$\eta_\pm = \frac{-6(\chi_1^2 - 3\chi_2) \pm \sqrt{36(\chi_1^2 - 3\chi_2)^2 - 120\chi_1\chi_3}}{60\chi_1^2}, \quad (54)$$

Equation (53) has no real solutions. Clearly, the acceptable part of the solution is that for $\eta \leq \eta_-$.

B. *C*1 integral equation

The unphysical loss of the solution for the percolation threshold as obtained from the virial expansion is present also in the isotropic SHS model ($\delta = \pi$). This shortcoming does not occur in an integral equation approach.[50] Within the Cn class of closures a crucial role is played by the angular average of the cavity function at contact $\bar{\bar{y}} = \langle y(r_{12} = \sigma, \Omega_1, \Omega_2, \Omega_{12})\epsilon^2(1,2)\rangle_{\Omega_1,\Omega_2,\Omega_{12}}$. Its density expansion reads

$$\bar{\bar{y}}^{\mathrm{Cn}} = y_0 + y_1\eta + y_2\eta^2 + \ldots, \quad (55)$$

where $y_n = y_n(\tau)$ is related to the reduced virial coefficients b_n by Eq. (41). For y_0 and y_1 they have already been computed in Eq. (33). The percolation threshold is then given by $\eta\bar{y}^{\mathrm{Cn}} = \tau$ where $\bar{y}^{\mathrm{Cn}} = \langle y^{\mathrm{Cn}}(r_{12} = \sigma, \Omega_1, \Omega_2, \Omega_{12})\epsilon(1,2)\rangle_{\Omega_1,\Omega_2,\Omega_{12}}$ and $y^{\mathrm{Cn}}(r_{12} = \sigma, \Omega_1, \Omega_2, \Omega_{12})$ is the contact cavity function within the Cn approximation.

Since $\epsilon^2 = \epsilon$ then $\bar{\bar{y}} = \bar{y}$ and within the *C*0 approximation ($\bar{y}^{C0} = y_0$) we find

$$\tau = \chi_1\eta, \quad (56)$$

whereas within the *C*1 approximation ($\bar{y}^{C1} = y_0 + y_1\eta$) we find

$$\eta = \frac{-6\chi_1\tau^2 + \sqrt{12}\tau^{3/2}\sqrt{\chi_3 + 3\chi_1^2\tau - 12\chi_2\tau + 30\chi_1\tau^2}}{\chi_3 - 12\chi_2\tau + 30\chi_1\tau^2}. \quad (57)$$

Now the loss of solution occurs between

$$\eta_\pm = \frac{-3(\chi_1^2 - 4\chi_2) \pm \sqrt{9(\chi_1^2 - 4\chi_2)^2 - 120\chi_1\chi_3}}{30\chi_1^2}. \quad (58)$$

Note that at small values of δ a gap may also appear in the *C*1 percolation threshold for $\delta \lesssim 1.21$ in the one-patch model and for $\delta \lesssim 1.22$ in the two-patch case. Figure 12 summarizes our findings and compares with MC simulations. From the figure we see that for δ close to π the percolation threshold of the two-patch model lies above that of the one-patch case at same total surface adhesive coverage, while the opposite trend is observed at lower δ. This mirrors our previous results for the coexistence curve.

Another quantity which is useful to assess the onset of a phase transition is the average coordination number, defined by

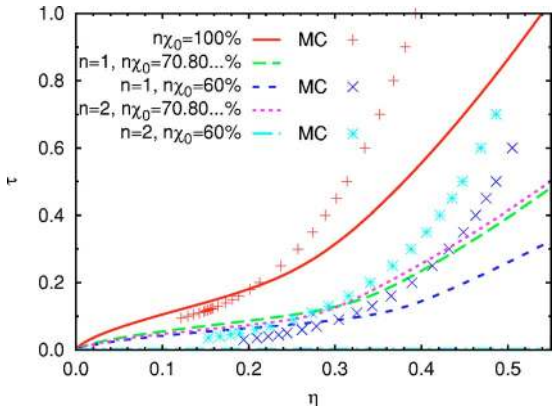

FIG. 12. (Color online) Percolation thresholds for various total adhesive coverages as calculated from the *C*1 approximation (lines), Eq. (57), and MC simulation (points). The one-patch ($n=1$) and two-patch ($n=2$) cases are compared at the same total coverage.

$$Z = \rho\int d\mathbf{r}_{12}\langle h^+(1,2)\rangle_{\Omega_1,\Omega_2,\Omega_{12}}. \quad (59)$$

One finds

$$Z = 2\frac{\eta}{\tau}\bar{y}^{\mathrm{Cn}}, \quad (60)$$

which on the percolation threshold gives $Z=2$. This prediction is compared with MC results in Fig. 13 where we show the average coordination number at the percolation threshold obtained from the MC simulations for the one- and two-patch models at 60% coverage.

We are now in a position to summarize the phase diagram for one and two patches within the *C*1 approximation. This is reported in Fig. 14. For two patches, the *C*1 phase diagram (coexistence curve and percolation line) is compared with MC results in Fig. 15 both for the full isotropic case (100% coverage) and for 60% coverage. Note that while the percolation line terminates at the point shown, the coexistence curve has a solution for the whole range of packing fraction considered. However, we have chosen to terminate the plot for the same value of η as the percolation line.

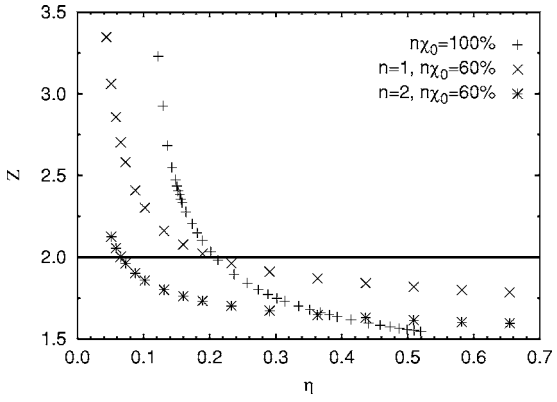

FIG. 13. Average coordination numbers at the percolation threshold for the one- and two-patch models at 60% coverage, obtained through MC. The continuous line is the prediction from the integral equation theory. The isotropic case is also reported for comparison.

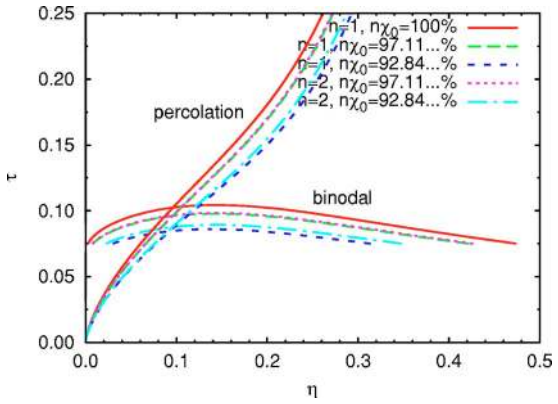

FIG. 14. (Color online) Phase diagram in the $C1$ approximation, for various values of the adhesive coverage $n\chi_0$. The one-patch ($n=1$) and two-patch ($n=2$) models are compared at the same total coverage.

VII. PHASE DIAGRAM AND ADDITION OF ADHESIVE BACKGROUND

So far we have considered the case of adhesive patches on hard spheres. The disadvantage of this model is that there is no fluid-fluid transition below a certain surface coverage χ_0. We have also shown that at fixed surface coverage the liquid more easily forms if the adhesion is distributed in different patches on the sphere surface for sufficiently large patches and we expect the opposite to be true for low coverage.

One could argue that a more physical model should have a strongly directional potential mimicking, e.g., active sites in a globular protein, in addition to an underlying isotropic attractive potential favoring a general fluid-fluid phase transition. To this aim, we modify our potential by adding a uniform adhesive background to each sphere on top of which a patchy potential of the type considered so far is active. This effect can be obtained by a simple substitution $\epsilon \rightarrow 1+\lambda\epsilon$ with λ measuring the strength of adhesion on the patches, yielding

$$\chi_1 \rightarrow 1 + \lambda\chi_1, \tag{61}$$

$$\chi_2 \rightarrow 1 + 2\lambda\chi_1 + \lambda^2\chi_2, \tag{62}$$

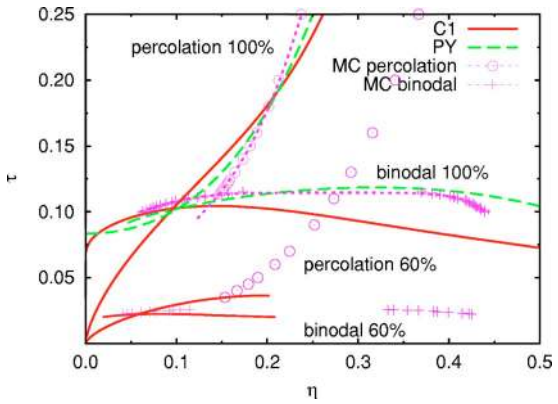

FIG. 15. (Color online) Comparison of the $C1$ approximation with MC simulation (dots) for the phase diagram of particles with two patches. The MC isotropic phase diagram is taken from Ref. 42.

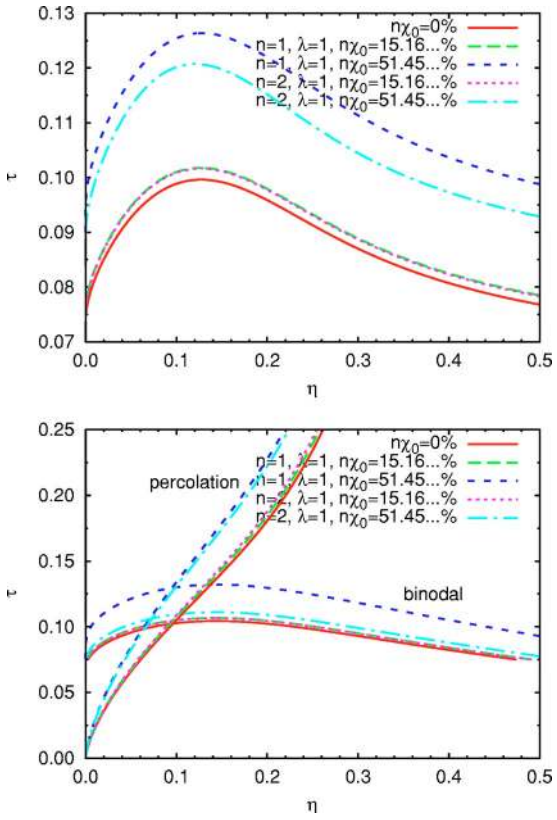

FIG. 16. (Color online) Dependence of the binodal line of patchy adhesive spheres with a background adhesion on the total surface coverage $n\chi_0$ of the patches: in the upper panel as calculated from the modified Carnahan–Starling free energy of Eq. (37); in the lower panel as calculated from the $C1$ approximation, Eq. (40).

$$\chi_3 \rightarrow 1 + 3\lambda\chi_1 + 3\lambda^2\bar{\chi}_2 + \lambda^3\chi_3, \tag{63}$$

where

$$\bar{\chi}_2 = \langle \epsilon(1,2)\epsilon(1,3)\rangle_{\Omega_1,\Omega_2,\Omega_3}\big|_{\theta_{12}=\pi/3}\ . \tag{64}$$

The phase diagram is now modified as depicted in Fig. 16 where we have set $\lambda=1$ to be the strength of the patches throughout. In this case we see that even a small sticky patch (of amplitude $\delta\sim 0.5$) is sufficient to raise both the binodal and percolation threshold of the isotropic model. At equal coverage, the binodal and percolation threshold of the two-patch model lie below their one-patch counterparts, in agreement with the observed trend in the absence of background adhesion.

Note that the critical point is now less sensitive to the size of the patches because an isotropic SHS—rather than a hard sphere—is now the limiting case as $\delta\rightarrow 0$. Indeed, the critical point does not move along η while it covers the whole range $\tau_c < \tau < 2\tau_c$ ($\lambda=1$), where τ_c is the critical reduced temperature of the isotropic model (see Fig. 17). The critical point shifts of the one- and two-patch models are now almost indistinguishable even though the crossing at 80% coverage still remains.

VIII. CONCLUSIONS

In this work we have studied, through integral equation theories and Monte Carlo simulations, the structure, percola-

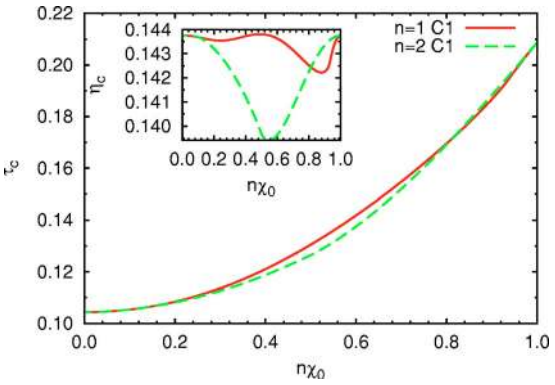

FIG. 17. (Color online) Dependence of the critical reduced temperature on the adhesive coverage in the patchy model with a uniform adhesive background, calculated from the $C1$ approximation, Eq. (40). The inset shows the behavior of the critical packing fraction.

tion, and fluid-fluid coexistence curves of a model of hard spheres with one or two uniform sticky patches on their surface. Particles interact through an adhesive Baxter potential only if patches on different spheres are suitably oriented and as hard spheres otherwise. Unlike most previous studies, we have been able to analyze in some detail the dependence of the aforementioned properties on the size of the patch and its interplay with the number of patches.

The integral equation theory is based on the first two approximations ($C0$ and $C1$) of a class of closures Cn which have already proved to provide a good qualitative representation of the exact behavior and are almost fully analytical. The comparison between the analytical work and Monte Carlo simulations indicates that $C1$ yields a gratifying qualitative description of the phase diagram notwithstanding the expected limitation due to its low density nature. While for the thermodynamics the results from the integral equation theories are exact within the given closure, for the percolation problem and the structure an additional orientational mean field approximation is necessary to decouple the orientational average.

Radial distribution functions within the $C0$ and $C1$ integral equation theories exhibit a characteristic jump at $r=2\sigma$ (whose magnitude depends on the patch angle δ) and a cusp at $r=3\sigma$. The coexistence and percolation lines move to lower temperature as the patch angle decreases from π (the isotropic case) to zero (hard spheres). For a fixed surface coverage above approximately 80%, the curves of the two-patch case lie above the corresponding single-patch ones, while the opposite trend is observed below that point. We have suggested that this is due to two patches of sufficiently large size being able to form bonds to more particles than can a single patch. We have also argued that this reasoning does not apply at low coverage, and that, in fact, the opposite situation might be expected. The crossover is not observed in the MC simulations within the range of adhesive coverage studied here (about 60%), but we cannot exclude the possibility for lower coverage, where the simulations converge very slowly. When an adhesive background is included in addition to the patches, both the liquid and percolating phase of the system are favored with respect to the isotropic case even in the presence of very small patches.

In spite of the limited number of cases (one or two patches) addressed in the present work, our analysis suggests that both the total fraction of the surface covered by adhesion and the number of patches are crucial parameters in controlling the location of the critical point. In the limit of a single bond per patch, our analysis is consistent with a recent suggestion[52] of a generalized law of corresponding states for anisotropic patchy interactions. We remark that, from the purely theoretical point of view, there exist only few paradigmatic toy models with anisotropic interactions amenable to analytical or semianalytical treatment.

Our analysis can be regarded as complementary to recent investigations of the phase diagrams of globular proteins[8,53,54] in that our starting point is the isotropic sticky hard sphere from which some adhesion is removed, rather than a hard sphere to which highly localized attractive spots are added. This approach goes beyond the limitation of one bond per patch, which is an essential feature of Wertheim thermodynamic perturbation theory. The price to pay is, of course, that only a qualitative agreement with MC simulations can be achieved.

It would be interesting to extend the present work in some respects. In view of the difficulties of MC simulations in probing low coverage, a comparison with a numerical solution of a more robust closure such as, for instance, the Percus–Yevick approximation which has a full analytical description in the isotropic case, would provide a more quantitative assessment of the results presented here. Such a solution would also help to evaluate the (uncontrolled) angular decoupling approximation exploited in the present analysis of structure and the percolation threshold. Work along these lines is in progress and will be presented in a future publication.

ACKNOWLEDGMENTS

This work was supported by the Italian MIUR (PRIN-COFIN 2006/2007). M.A.M. thanks the Royal Society of London and EPSRC (United Kingdom) for financial support.

APPENDIX A: THE LAW OF CORRESPONDING STATES

Consider the simplest possible dependence $\Delta(\hat{\mathbf{s}}_1,\hat{\mathbf{s}}_2)=\hat{\mathbf{s}}_1\cdot\hat{\mathbf{s}}_2$ and assume that $\epsilon(1,2)=\Delta(\hat{\mathbf{s}}_1,\hat{\mathbf{s}}_2)$, i.e., the adhesion coefficient does not depend on $\hat{\mathbf{r}}_{12}=\mathbf{r}_{12}/r_{12}$. Within the Weeks–Chandler–Andersen perturbative expansion[55] of the Helmholtz free energy A^{SHS} one finds

$$\frac{\beta(A^{\mathrm{SHS}}-A^{\mathrm{HS}})}{N}=\int d(1)d(2)a^{(1)}(\mathbf{r}_1,\mathbf{r}_2;\eta)\Delta e(1,2)+\int d(1)d(2)d(3)d(4)\times a^{(2)}(\mathbf{r}_1,\mathbf{r}_2,\mathbf{r}_3,\mathbf{r}_4;\eta)\Delta e(1,2)\Delta e(3,4)+\ldots, \tag{A1}$$

where $d(i)$ is a short-hand notation for $d\mathbf{r}_i d\tilde{\Omega}_i$, with $d\tilde{\Omega}_i$ the average solid angle $\sin\theta_i d\theta_i d\varphi_i/(4\pi)$, A^{HS} the Helmholtz free energy of the reference hard sphere (HS) system

$$\Delta e(1,2) = \frac{\epsilon(1,2)}{12\tau}\delta(r_{12}-\sigma), \tag{A2}$$

and the functions $a^{(n)}$ are expressed in terms of the correlation functions of the reference system which only depend on the packing fraction $\eta=\pi\rho\sigma^3/6$, with ρ as the density. We see then that the angular dependence in ϵ factorizes and one finds

$$\frac{\beta(A^{\mathrm{SHS}}-A^{\mathrm{HS}})}{N} = \sum_i A^{(i)}(\eta)\left(\frac{\chi_1}{12\tau}\right)^i, \tag{A3}$$

where $\chi_1=\int d\tilde{\Omega}_1 d\tilde{\Omega}_2 \epsilon(1,2)$. This analysis shows how, in this case, the law of corresponding states holds. For example, if $\tau=g(\eta)$ is the spinodal or binodal of the SHS system with isotropic interaction ($\epsilon=1$),[27,56,57] then the spinodal or binodal of the SHS with directional adhesion will be $\tau=\chi_1 g(\eta)$, which will lie above that of the isotropic system if $\chi_1>1$ and below otherwise.

APPENDIX B: THE THIRD VIRIAL COEFFICIENT

In this appendix we provide a derivation of Eqs. (6)–(9). We start from the usual definition of the third virial coefficient

$$B_3 = -\frac{1}{3V}\int d\mathbf{r}_1 d\mathbf{r}_2 d\mathbf{r}_3 \langle f(1,2)f(1,3)f(2,3)\rangle_{\Omega_1,\Omega_2,\Omega_3}, \tag{B1}$$

where, in line with Eq. (2), the Mayer function can split into two terms

$$f(i,j) = f_{\mathrm{HS}}(i,j) + \frac{\sigma}{12\tau}\epsilon(i,j)\delta(r_{ij}-\sigma). \tag{B2}$$

In the earlier equation we have set the HS part to the usual form

$$f_{\mathrm{HS}}(i,j) = -\Theta(\sigma-r_{ij}). \tag{B3}$$

Upon expanding the product, one can easily find

$$\Delta B_3 = B_3 - B_3^{\mathrm{HS}} = \Delta B_3^{(1)} + \Delta B_3^{(2)} + \Delta B_3^{(3)}, \tag{B4}$$

where $B_3^{\mathrm{HS}}=5\pi^2\sigma^6/18$ is the HS result and

$$\Delta B_3^{(1)} = -\frac{1}{V}\left(\frac{\sigma}{12\tau}\right)\int d\mathbf{r}_1 d\mathbf{r}_2 d\mathbf{r}_3 \langle f_{\mathrm{HS}}(1,2)f_{\mathrm{HS}}(1,3) \times \epsilon(2,3)\delta(r_{23}-\sigma)\rangle_{\Omega_1,\Omega_2,\Omega_3}, \tag{B5}$$

$$\Delta B_3^{(2)} = -\frac{1}{V}\left(\frac{\sigma}{12\tau}\right)^2\int d\mathbf{r}_1 d\mathbf{r}_2 d\mathbf{r}_3 \langle f_{\mathrm{HS}}(1,2) \times \epsilon(1,3)\delta(r_{13}-\sigma)\epsilon(2,3)\delta(r_{23}-\sigma)\rangle_{\Omega_1,\Omega_2,\Omega_3}, \tag{B6}$$

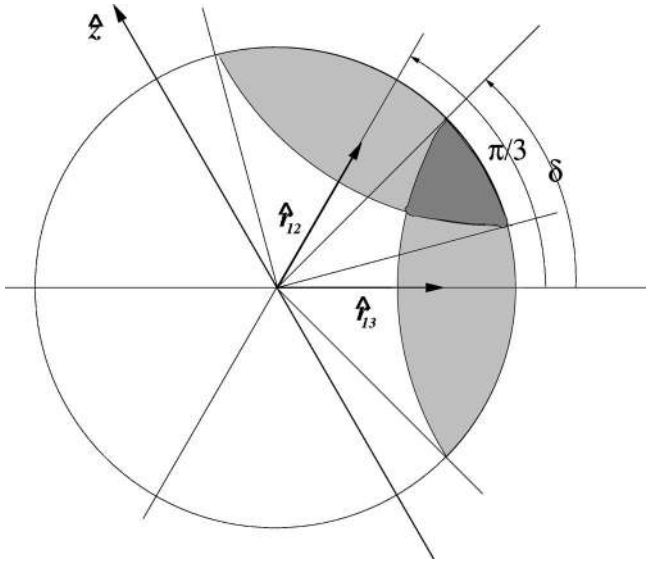

FIG. 18. Basic geometry for the calculation of $R_1(\delta)$ in Eq. (C1). The required solid angle is the overlap of the two cones of width δ (the darkly shaded region in the sketch).

$$\Delta B_3^{(3)} = -\frac{1}{3V}\left(\frac{\sigma}{12\tau}\right)^3\int d\mathbf{r}_1 d\mathbf{r}_2 d\mathbf{r}_3 \langle \epsilon(1,2)\delta(r_{12}-\sigma) \times \epsilon(1,3)\delta(r_{13}-\sigma)\epsilon(2,3)\delta(r_{23}-\sigma)\rangle_{\Omega_1,\Omega_2,\Omega_3}. \tag{B7}$$

The earlier integrals are most conveniently evaluated in bipolar coordinates by introducing $\mathbf{r}_{12}=\mathbf{r}_2-\mathbf{r}_1$ and $\mathbf{r}_{13}=\mathbf{r}_3-\mathbf{r}_1$. This leads to $r_{23}=\sqrt{r_{12}^2+r_{13}^2-2r_{12}r_{13}\hat{\mathbf{r}}_{12}\cdot\hat{\mathbf{r}}_{13}}$ where it is most convenient to choose $\hat{\mathbf{r}}_{13}$ as the z axis. For $\Delta B_3^{(1)}$ one finds

$$\Delta B_3^{(1)} = -\left(\frac{\sigma}{12\tau}\right)\int d\mathbf{r}_{23} d\mathbf{r}_{12}\Theta(\sigma-r_{12})\Theta(\sigma-|\mathbf{r}_{12}-\mathbf{r}_{23}|) \times \delta(r_{23}-\sigma)\langle\epsilon(2,3)\rangle_{\Omega_2,\Omega_3}. \tag{B8}$$

Here one first performs the integration over $\mathbf{r}_{12}$, which covers twice a spherical cap of height $\sigma/2$ and then the straightforward integration over $\mathbf{r}_{23}$. Clearly the anisotropic part decouples, thus yielding the isotropic part times χ_1 as claimed. For $\Delta B_3^{(2)}$ a little more care is necessary. One first obtains

$$\Delta B_3^{(2)} = \left(\frac{\sigma}{12\tau}\right)^2\int_0^\infty dr_{12} r_{12}^2\Theta(\sigma-r_{12}) \times \int_0^\infty dr_{13} r_{13}^2\delta(\sigma-r_{13})\int d\Omega_{12} d\Omega_{13} \times \delta(\sqrt{r_{12}^2+r_{13}^2-2r_{12}r_{13}\cos\theta_{12}}-\sigma) \times \langle\epsilon(1,3)\epsilon(2,3)\rangle_{\Omega_1,\Omega_2,\Omega_3}. \tag{B9}$$

After a first integration over r_{13}, an additional integration over $\cos\theta_{12}$ then requires $\theta_{13}\leq\pi/3$ (corresponding to the maximum available angle for all three particles in reciprocal contact). This also yields a normalization factor $4=1/\sin^2(\pi/6)$ in order to have the correct limit $\epsilon(i,j)\to 1$ for all (i,j). The final result is

$$\Delta B_3^{(2)} = \frac{\pi^2\sigma^6}{36\tau^2}\frac{1}{4\pi}\int d\Omega_{13} \times 4\left\langle \epsilon(1,2)\epsilon(2,3)\Theta\left(\frac{\pi}{3}-\theta_{13}\right)\right\rangle_{\Omega_1,\Omega_2,\Omega_3}, \quad \text{(B10)}$$

thus yielding the isotropic part times χ_2 as reported in Eq. (8). An almost identical procedure also gives

$$\Delta B_3^{(3)} = -\left(\frac{\sigma}{12\tau}\right)^3\frac{8\pi^2\sigma^2}{3}\int_0^\infty dr_{12}r_{12}^2\delta(r_{12}-\sigma) \times\int_{-1}^{+1} d(\cos\,\theta_{12})\,\delta(\sqrt{r_{12}^2+\sigma^2-2r_{12}\sigma\cos\,\theta_{12}}-\sigma) \times\langle\epsilon(1,2)\epsilon(1,3)\epsilon(2,3)\rangle_{\Omega_1,\Omega_2,\Omega_3}, \quad \text{(B11)}$$

which, after an integration over the angular variables, leads to the desired decoupling for the anisotropic part χ_3 as given in Eq. (9). Note that in this configuration all three spheres are necessarily touching and this fixes the angles θ_{ij} to a well defined value given in Eq. (9). This completes the derivation of Eq. (6).

APPENDIX C: COEFFICIENTS χ_2 AND χ_3 FOR THE ONE-PATCH CASE

Here we give the analytic expressions for the coefficients Q_1 and R_1 used in Eqs. (12) and (13) of the main text in terms of characteristic integrals which are then evaluated numerically. The basic procedure follows a similar analysis carried out in a different context,[58] which requires the calculation of the solid angle associated with the intersection of two identical patches on the same sphere as indicated in Fig. 18. For χ_3, one can easily see that for $\delta<\pi/6$ there is no possibility of intersection, even in the close-packed configuration. For $\delta\geq\pi/6$ the form of the resulting integral can be most conveniently written in slightly different ways depending on the amplitude δ of the patch

$$R_1(\delta) = \alpha_{b,1}(\delta)\Theta\left(\delta-\frac{\pi}{6}\right)\Theta\left(\frac{2\pi}{3}-\delta\right) + \beta_{b,1}(\delta)\Theta\left(\delta-\frac{2\pi}{3}\right)\Theta\left(\frac{5\pi}{6}-\delta\right) + \gamma_{b,1}(\delta)\Theta\left(\delta-\frac{5\pi}{6}\right), \quad \text{(C1)}$$

where the various terms are given in terms of the integrals

$$\alpha_{b,1}(\delta) = \frac{1}{\pi}\int_{2\pi/3-\delta}^{\pi/2} d\theta\,\sin\,\theta\,\arccos\left(\frac{\cos\,\delta-\,\cos\,\theta\cos\,2\pi/3}{\sin\,\theta\sin\,2\pi/3}\right), \quad \text{(C2)}$$

$$\beta_{b,1}(\delta) = 1-\frac{1}{\pi}\int_{\delta-2\pi/3}^{\pi/2} d\theta\,\sin\,\theta\,\arccos\left(\frac{\cos(\pi-\delta)-\,\cos\,\theta\cos\,\pi/3}{\sin\,\theta\sin\,\pi/3}\right), \quad \text{(C3)}$$

$$\gamma_{b,1}(\delta) = 1-2\,\sin^2\left(\frac{\pi-\delta}{2}\right). \quad \text{(C4)}$$

For example $\alpha_{b,1}$ given in Eq. (C2) is the simplest integral resulting from the calculation of the overlapping region of the two cones of width δ as depicted in Fig. 18.

For χ_2 an additional complication arises from the additional degree of freedom given by the fact that only two of the three spheres are (in general) in contact. One finds

$$Q_1(\delta) = \alpha_{a,1}(\delta)\Theta\left(\frac{\pi}{6}-\delta\right) + \beta_{a,1}(\delta)\Theta\left(\delta-\frac{\pi}{6}\right)\Theta\left(\frac{\pi}{2}-\delta\right) + \gamma_{a,1}(\delta)\Theta\left(\delta-\frac{\pi}{2}\right)\Theta\left(\frac{5\pi}{6}-\delta\right) + \delta_{a,1}(\delta)\Theta\left(\delta-\frac{5\pi}{6}\right), \quad \text{(C5)}$$

with

$$\alpha_{a,1}(\delta) = \frac{2}{\pi}\int_0^{2\delta} d\theta'\,\sin\,\theta'\int_{\pi/2+\theta'/2-\delta}^{\pi/2} d\theta\,\sin\,\theta\,\arccos\left(\frac{\cos\,\delta-\cos\,\theta\cos(\pi/2+\theta'/2)}{\sin\,\theta\sin(\pi/2+\theta'/2)}\right), \quad \text{(C6)}$$

$$\beta_{a,1}(\delta) = \frac{2}{\pi}\int_0^{\pi/3} d\theta'\,\sin\,\theta'\int_{\pi/2+\theta'/2-\delta}^{\pi/2} d\theta\,\sin\,\theta\,\arccos\left(\frac{\cos\,\delta-\cos\,\theta\cos(\pi/2+\theta'/2)}{\sin\,\theta\sin(\pi/2+\theta'/2)}\right), \quad \text{(C7)}$$

$$\gamma_{a,1}(\delta) = \frac{2}{\pi}\left[\frac{\pi}{2}-\int_0^{\pi/3} d\theta'\,\sin\,\theta'\int_{\delta-\pi/2-\theta'/2}^{\pi/2} d\theta\,\sin\,\theta\,\arccos\left(\frac{\cos(\pi-\delta)-\cos\,\theta\cos(\pi/2-\theta'/2)}{\sin\,\theta\sin(\pi/2-\theta'/2)}\right)\right], \quad \text{(C8)}$$

$$\delta_{a,1}(\delta)=\frac{2}{\pi}\left\{2\pi\sin^2\delta+\int_0^{2(\pi-\delta)}d\theta'\sin\theta'\int_{\delta-\pi/2-\theta'/2}^{\pi/2}d\theta\sin\theta\arccos\left(\frac{\cos(\pi-\delta)-\cos\theta\cos(\pi/2-\theta'/2)}{\sin\theta\sin(\pi/2-\theta'/2)}\right)\right.$$
$$\left.+\left[1-2\sin^2\left(\frac{\pi-\delta}{2}\right)\right]\frac{\pi}{2}[2\cos(2\delta)-1]\right\}. \tag{C9}$$

APPENDIX D: COEFFICIENTS χ_2 AND χ_3 FOR THE TWO-PATCH CASE

Here we give the analytic expressions for the coefficients Q_2 and R_2 used in Eqs. (15) and (16) of the main text

$$Q_2(\delta)=\alpha_{a,2}(\delta)\Theta\left(\frac{\pi}{6}-\delta\right)+\beta_{a,2}(\delta)\Theta\left(\delta-\frac{\pi}{6}\right)\Theta\left(\frac{\pi}{3}-\delta\right)+\gamma_{a,2}(\delta)\Theta\left(\delta-\frac{\pi}{3}\right)\Theta\left(\frac{\pi}{2}-\delta\right), \tag{D1}$$

$$R_2(\delta)=\alpha_{b,2}(\delta)\Theta\left(\delta-\frac{\pi}{6}\right)\Theta\left(\frac{\pi}{3}-\delta\right)+\beta_{b,2}(\delta)\Theta\left(\delta-\frac{\pi}{3}\right)\Theta\left(\frac{\pi}{2}-\delta\right), \tag{D2}$$

with

$$\alpha_{a,2}(\delta)=\frac{4}{\pi}\int_0^{2\delta}d\theta'\sin\theta'\int_{\pi/2+\theta'/2-\delta}^{\pi/2}d\theta\sin\theta\arccos\left(\frac{\cos\delta-\cos\theta\cos(\pi/2+\theta'/2)}{\sin\theta\sin(\pi/2+\theta'/2)}\right), \tag{D3}$$

$$\beta_{a,2}(\delta)=\frac{4}{\pi}\int_0^{\pi/3}d\theta'\sin\theta'\int_{\pi/2+\theta'/2-\delta}^{\pi/2}d\theta\sin\theta\arccos\left(\frac{\cos\delta-\cos\theta\cos(\pi/2+\theta'/2)}{\sin\theta\sin(\pi/2+\theta'/2)}\right), \tag{D4}$$

$$\gamma_{a,2}(\delta)=\frac{4}{\pi}\left[\int_0^{\pi/3}d\theta'\sin\theta'\int_{\pi/2+\theta'/2-\delta}^{\pi/2}d\theta\sin\theta\arccos\left(\frac{\cos\delta-\cos\theta\cos(\pi/2+\theta'/2)}{\sin\theta\sin(\pi/2+\theta'/2)}\right)\right.$$
$$\left.+\int_0^{\pi/3}d\theta'\sin\theta'\int_{\pi/2}^{\theta'/2+\delta}d\theta\sin\theta\arccos\left(\frac{\cos\delta-\cos\theta\cos(\theta'/2)}{\sin\theta\sin(\theta'/2)}\right)\right], \tag{D5}$$

$$\alpha_{b,2}(\delta)=\frac{2}{\pi}\int_{2\pi/3-\delta}^{\pi/2}d\theta\sin\theta\arccos\left(\frac{\cos\delta-\cos\theta\cos 2\pi/3}{\sin\theta\sin 2\pi/3}\right), \tag{D6}$$

$$\beta_{b,2}(\delta)=\frac{2}{\pi}\int_{2\pi/3-\delta}^{\pi/2}d\theta\sin\theta\arccos\left(\frac{\cos\delta-\cos\theta\cos 2\pi/3}{\sin\theta\sin 2\pi/3}\right)+\frac{2}{\pi}\int_{\pi/2}^{\pi/6+\delta}d\theta\sin\theta\arccos\left(\frac{\cos\delta-\cos\theta\cos\pi/6}{\sin\theta\sin\pi/6}\right). \tag{D7}$$

[1] L. Boltzmann, *Lectures on Gas Theory* (Dover, New York, 1995), Chap. 6.
[2] G. Jackson, W. G. Chapman, and K. E. Gubbins, Mol. Phys. **65**, 1 (1988).
[3] L. Blum, P. T. Cummings, and D. Bratko, J. Chem. Phys. **92**, 3741 (1990).
[4] N. A. Busch, M. S. Wertheim, Y. C. Chiew, and M. L. Yarmush, J. Chem. Phys. **101**, 3147 (1994).
[5] D. Ghonasgi and W. G. Chapman, J. Chem. Phys. **102**, 2585 (1995).
[6] N. A. Busch, M. S. Wertheim, and M. L. Yarmush, J. Chem. Phys. **104**, 3962 (1996).
[7] A. Lomakin, N. Asherie, and G. B. Benedek, Proc. Natl. Acad. Sci. U.S.A. **96**, 9465 (1999).
[8] R. P. Sear, J. Chem. Phys. **111**, 4800 (1999).
[9] E. Mileva and G. T. Evans, J. Chem. Phys. **113**, 3766 (2000).
[10] F. Sciortino, Nat. Mater. **1**, 145 (2002).
[11] F. W. Starr and J. F. Douglas, J. Chem. Phys. **119**, 1777 (2003).
[12] N. Kern and D. Frenkel, J. Chem. Phys. **118**, 9882 (2003).
[13] Z. Zhang and S. C. Glotzer, Nano Lett. **4**, 1407 (2004).
[14] S. C. Glotzer, Science **306**, 419 (2004).
[15] Y. S. Cho, G. R. Yi, J. M. Lim, S. H. Kim, V. N. Maniharan, D. J. Pine, and S. M. Yang, J. Am. Chem. Soc. **127**, 15968 (2005).
[16] F. Sciortino, P. Tartaglia, and E. Zaccarelli, J. Phys. Chem. B **109**, 21942 (2005).
[17] E. Bianchi, J. Largo, P. Tartaglia, E. Zaccarelli, and F. Sciortino, Phys. Rev. Lett. **97**, 168301 (2006).
[18] M. F. Hagan and D. Chandler, Biophys. J. **91**, 42 (2006).
[19] A. W. Wilber, J. P. K. Doye, A. A. Louis, E. G. Noya, M. A. Miller, and P. Wong, J. Chem. Phys. **127**, 085106 (2007).
[20] M. Wertheim, J. Stat. Phys. **35**, 19 (1984).
[21] Yu. V. Kalyuzhnyi, M. F. Holovko, and A. D. J. Haymet, J. Chem. Phys. **95**, 9151 (1991).
[22] Yu. V. Kalyuzhnyi, G. Stell, M. L. Llano-Rastrepo, W. G. Chapman, and M. F. Holovko, J. Chem. Phys. **101**, 7939 (1994).
[23] R. Piazza, V. Peyre, and V. Degiorgio, Phys. Rev. E **58**, R2733 (1998).
[24] A. Giacometti, D. Gazzillo, G. Pastore, and T. K. Das, Phys. Rev. E **71**, 031108 (2005).
[25] G. Pellicane, D. Costa, and C. Caccamo, J. Phys. Chem. B **108**, 7538 (2004).
[26] A. Lomakin, N. Asherie, and G. B. Benedek, J. Chem. Phys. **104**, 1646 (1996).
[27] R. J. Baxter, J. Chem. Phys. **49**, 2770 (1968).
[28] G. Stell, J. Stat. Phys. **63**, 1203 (1991).
[29] P. Charbonneau and D. Frenkel, J. Chem. Phys. **126**, 196101 (2007).
[30] C. G. Gray and K. E. Gubbins, *Theory of Molecular Fluids* (Clarendon, New York, 1984).

[31] L. Blum and A. J. Torruella, J. Chem. Phys. **56**, 303 (1972).
[32] L. Blum, J. Chem. Phys. **57**, 1862 (1972).
[33] L. Blum, J. Chem. Phys. **58**, 3295 (1973).
[34] M. S. Wertheim, J. Chem. Phys. **55**, 4291 (1971).
[35] D. Gazzillo, R. Fantoni, and A. Giacometti (unpublished).
[36] D. Gazzillo and A. Giacometti, J. Chem. Phys. **120**, 4742 (2004).
[37] M. A. Miller and D. Frenkel (unpublished).
[38] N. A. Seaton and E. D. Glandt, J. Chem. Phys. **87**, 1785 (1987).
[39] W. G. T. Kranendonk and D. Frenkel, Mol. Phys. **64**, 403 (1988).
[40] A. Jamnik and D. Bratko, Phys. Rev. E **50**, 1151 (1994).
[41] M. A. Miller and D. Frenkel, J. Chem. Phys. **121**, 535 (2004).
[42] M. A. Miller and D. Frenkel, Phys. Rev. Lett. **90**, 135702 (2003).
[43] J. W. Perram, Mol. Phys. **30**, 1505 (1975).
[44] P. T. Cummings, J. W. Perram, and W. R. Smith, Mol. Phys. **31**, 535 (1976).
[45] M. A. Miller and D. Frenkel, J. Phys.: Condens. Matter **16**, S4901 (2004).
[46] F. Romano, P. Tartaglia, and F. Sciortino, J. Phys.: Condens. Matter **19**, 322101 (2007).
[47] R. Fantoni, D. Gazzillo, A. Giacometti, and P. Sollich, J. Chem. Phys. **125**, 164504 (2006).
[48] N. F. Carnahan and K. E. Starling, J. Chem. Phys. **51**, 635 (1969).
[49] B. J. Alder and T. E. Wainwright, J. Chem. Phys. **27**, 1208 (1957).
[50] R. Fantoni, D. Gazzillo, and A. Giacometti, J. Chem. Phys. **122**, 034901 (2005).
[51] U. Alon, A. Drory, and I. Balberg, Phys. Rev. A **42**, 4634 (1990).
[52] G. Foffi and F. Sciortino, J. Phys. Chem. B **111**, 9702 (2007).
[53] P. R. ten Wolde and D. Frenkel, Science **277**, 1975 (1997).
[54] J. F. Lutsko and G. Nicolis, J. Chem. Phys. **122**, 244907 (2005).
[55] H. C. Andersen, J. D. Weeks, and D. Chandler, Phys. Rev. A **4**, 1597 (1971).
[56] R. J. Baxter, in *Physical Chemistry, an Advanced Treatise*, edited by D. Henderson (Academic, New York, 1971), Vol. 8A, Chap. 4.
[57] R. O. Watts, D. Henderson, and R. J. Baxter, Adv. Chem. Phys. **21**, 421 (1971).
[58] S. M. Oversteegen and H. N. W. Lekkerkerker, Phys. Rev. E **68**, 021404 (2003).